Heliyon 5 (2019) e02238

Contents lists available at ScienceDirect

Heliyon

journal homepage: www.heliyon.com

On the discovery of a potential survivin inhibitor combining computational tools and cytotoxicity studies

Patricia A. Quispe, Martin J. Lavecchia **, Ignacio E. León *

CEQUINOR (Centro de Química Inorgánica, CONICET-UNLP) Facultad de Ciencias Exactas, Universidad Nacional de La Plata, 1900, La Plata, Argentina

ARTICLE INFO

Keywords:
Molecular biology
Computational biology
Bioinformatics
Survivin
Inhibitors
Docking studies
Molecular dynamics

ABSTRACT

Survivin protein is a metalloprotein member of the inhibitors of apoptosis proteins family, involved in the regulation of programmed cell death. Due to the recent development of antitumor therapies having survivin as molecular target, several strategies to interfere with the expression or function of survivin have emerged. This work describes the discovery of a new potential inhibitor of survivin function using a computer-aided drug design approach. Structure-based virtual screening and molecular dynamic simulations were carried out to select two compounds as possible inhibitors. According to the binding energy, possible ligand localization is in a cavity, close to dimerization interface. Next, cell-based assays were performed on three cell lines: two with tumor phenotype and over-expression of survivin, and another with normal phenotype and low expression of survivin. One of the selected compounds shows a selectively antitumor effect on panel cell lines suggesting that the compound effect could be correlated with the survivin expression.

1. Introduction

Survivin protein (16,5 kDa) is a metalloprotein member of the inhibitors of apoptosis protein (IAP) family, involved in the regulation of programmed cell death [1]. Encoded by the BIRC5 gene located at the 17q25 locus in humans [2]. Wild-type survivin protein has 142 amino acids although there are variants of alternative splicing with a flexible amount of amino acids and unknown functions [3].

The survivin structure has a single repetition of the BIR (Baculovirus IAP repeat) domain of approximately 70 amino acids at its N-terminus, characteristic of IAPs. Unlike other IAPs, it lacks the RING finger domain carboxy-terminal and instead it has a long alpha-helix coil of 40 amino acids and 65Å involved in the association of the protein with the microtubules during the G2/M phase of the cell cycle. This domain is key to the interaction with the components of the chromosomal passage complex, during late mitosis [4, 5]. Regarding its behavior, crystallographic studies have shown that it forms homodimers across the interface of dimerization, which includes the residues 6–10 and 89–102. The dimeric structure is stabilized by the formation of non-polar contacts between residues, mostly hydrophobic, with a total contact area between monomers of around 500Å^2 [4, 6]. It is expressed mainly in embryonic tissues [2] and has a significant role in regulation of cell division and cell survival [4, 7, 8]. However, its expression levels decrease during development, being undetectable in terminally differentiated normal tissues [2, 5]. Nevertheless, survivin expression is upregulated in many types of tumors in which increases cell survival and tumor progression, mainly due to the inhibition of apoptosis [9]. Additionally, upregulation of survivin correlates with a poor response to chemotherapy and a poor clinical prognosis in patients with lung, bone, colon, breast, and stomach cancer [10, 11].

Otherwise, downregulation of survivin expression is related to an increase in the activity of caspase-3 and enhanced apoptosis in human cervix cancer cell line [5, 7]. In addition, downregulation of survivin expression has been shown to enhance the efficacy of cytotoxic drugs, increasing the sensitivity of tumors cells on in vitro and in vivo conditions [12, 13, 14]. This shows the relevance of the development of anti-tumor therapies by selecting survivin as molecular target.

In recent years, several strategies have been developed to interfere with the expression or function of survivin, among which the use of small interfering RNA, antisense oligonucleotides, dominant-negative mutant, vaccine-based therapies and use of small molecules inhibitors [15, 16]. For example, Mir-335 [17] and **LY2181308** are small interfering RNAs that destabilize survivin mRNA and induce its degradation [18]. Moreover, different small molecules as YM155 [19, 20, 21] and FL118 [18,22]

* Corresponding author.
** Corresponding author.
E-mail addresses: lavecchia@quimica.unlp.edu.ar (M.J. Lavecchia), ileon@biol.unlp.edu.ar (I.E. León).

https://doi.org/10.1016/j.heliyon.2019.e02238
Received 15 January 2019; Received in revised form 26 June 2019; Accepted 2 August 2019

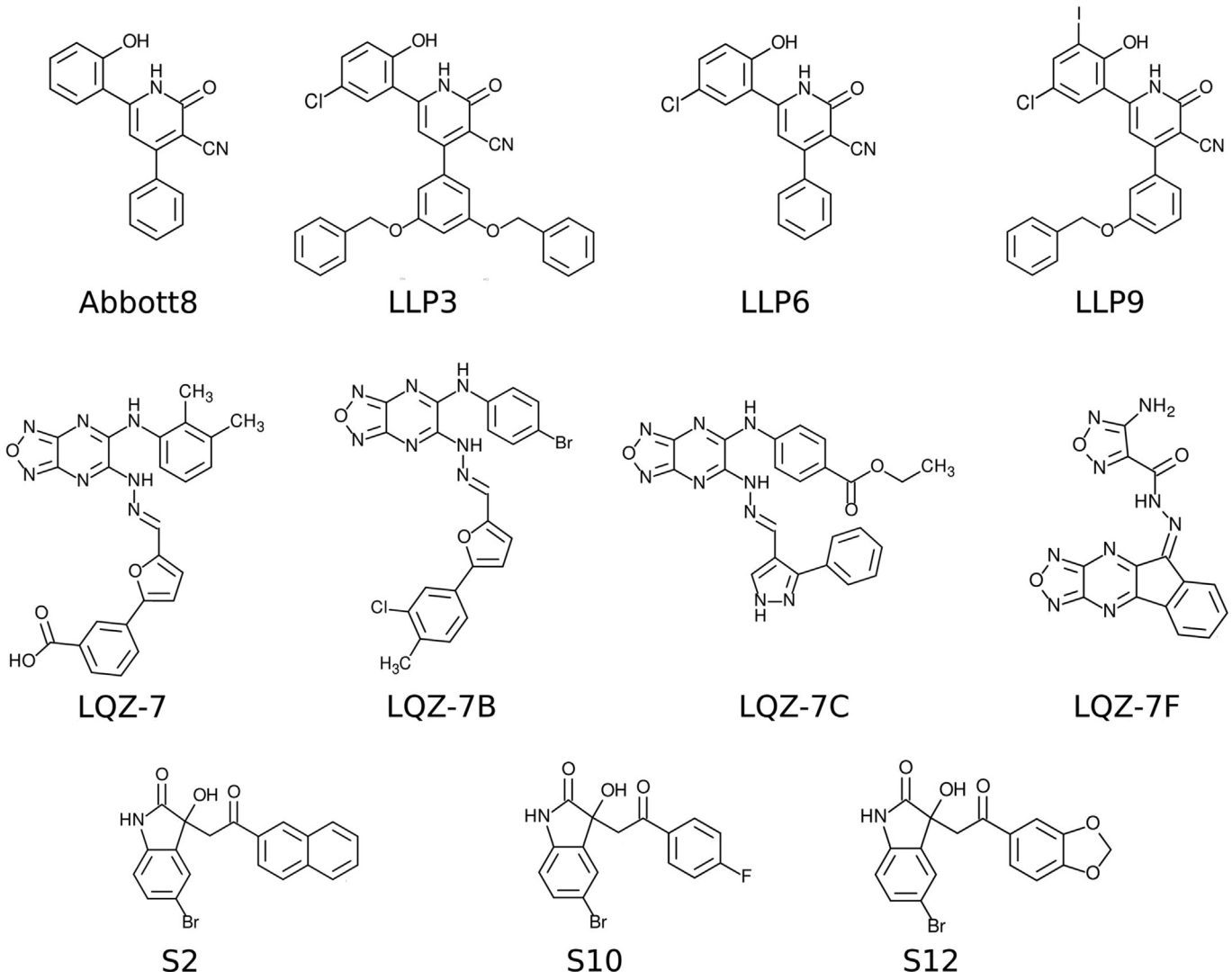

Fig. 1. Schemes of the molecules included in the docking validation that are known to have interaction with survivin.

block the transcription of the BIRC5 gene. In recent years, the development of inhibitors that interact directly with the protein emerged. This has been a challenge since survivin is considered a "non-druggable" protein for not having catalytic activity or natural ligands, and its function is mediated by protein-protein interactions [23, 24, 25]. However, some ligand-binding sites in survivin have been proposed for the inhibition of their function, established through affinity-based techniques and *in-silico* methods [26, 27, 28]. In this sense, the small molecule **Abbott8** (Fig. 1) was identified by high-throughput screening (HTS), which interacts with a cavity, next to the dimerization interface [29, 30]. In addition, structural analogues of **Abbott8** (**LLP3**, **LLP6**, **LLP9,** see Fig. 1) exhibited antitumor activity [28] and docking studies have shown that these compounds also interact in this cavity. Also, Berezov et al. reported novel ligands (**S2**, **S10**, **S12,** see Fig. 1**)** that interact in the cavity, slightly further away from the dimerization interface with respect to **Abbott**. **S12** has shown in vitro and in vivo antitumor activity in cancer cell lines that overexpress survivin and in xenographic pancreatic models [27]. Berezov et al. proposed this cavity as a binding site for the potential ligands capable of inducing allosteric conformational changes and modulating the function of survivin. On the other hand, **LQZ-7** and derivative compounds (**LQZ-7B**, **LQZ-7C** and **LQZ-7F**) (Fig. 1) have been shown effectively to disrupt the dimer form of survivin and induce programmed cell death and inhibition of proteasome activity [26]. In this case, Qi et al. proposed using docking that the interaction occurs in the dimerization interface.

Here, we describe the discovery of new potential inhibitors of survivin function, using a computer-aided drug design approach. Structure-based virtual screening (SBVS) and molecular dynamics were carried out to select two compounds as possible inhibitors. Next, cell-based assays were performed on three cell lines: two with tumor phenotype and over-expression of survivin, and another with normal phenotype and low expression of survivin. Finally, one of the selected compounds, **ZINC2243688**, shows a selective antitumor effect on panel cell lines suggesting that the compound effect could be correlated with survivin expression.

2. Materials and methods

2.1. Materials

Tissue culture materials were purchased from Corning (Princeton, NJ, USA), Dulbecco's modified Eagle's medium (DMEM) and TrypLE ^{TM} were purchased from Gibco (Gaithersburg, MD, USA), and fetal bovine serum (FBS) was purchased from Internegocios (Argentina).

2-(3-hydroxyphenyl)benzo[h]chromen-4-one **(ZINC57885)** and (1S,3R)-3-((((9H-Fluoren-9-yl) methoxy)carbonyl)amino)cyclopentanecarboxylic acid **(ZINC2243688)** were purchased from Sigma (St. Louis, MO, USA).

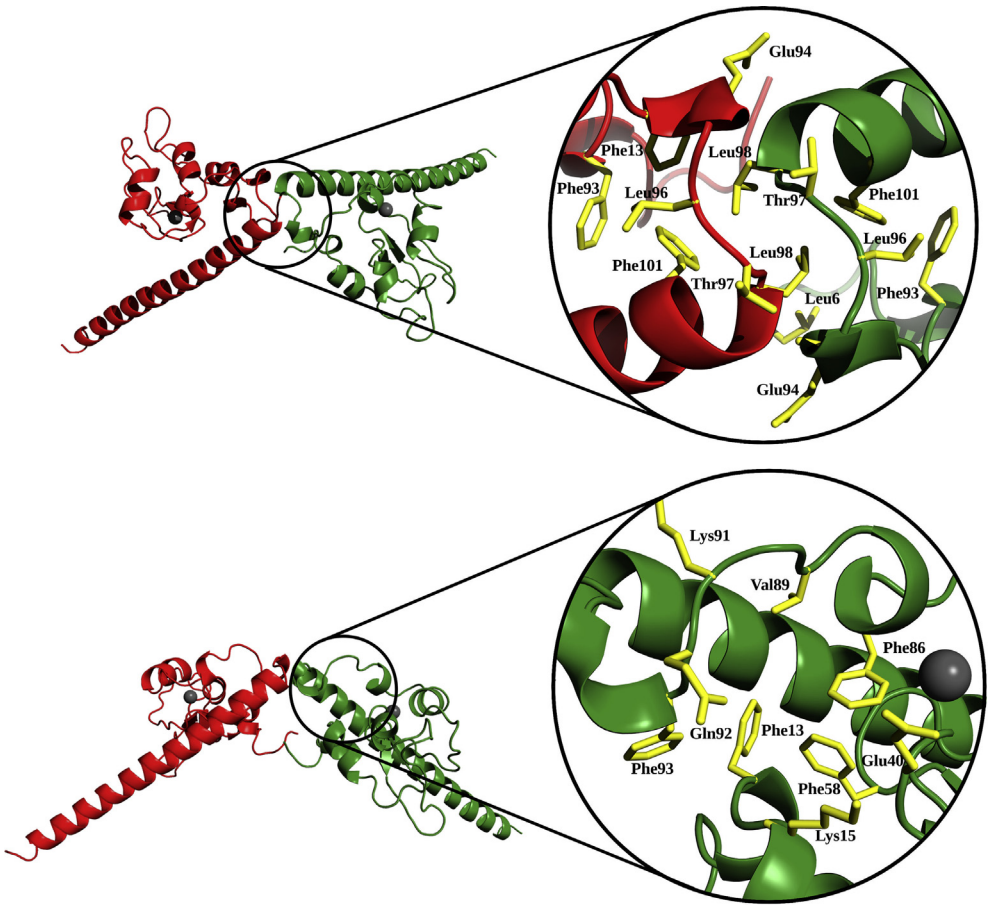

Fig. 2. Detailed view of dimerization interface (above) and hydrophobic cavity (below).

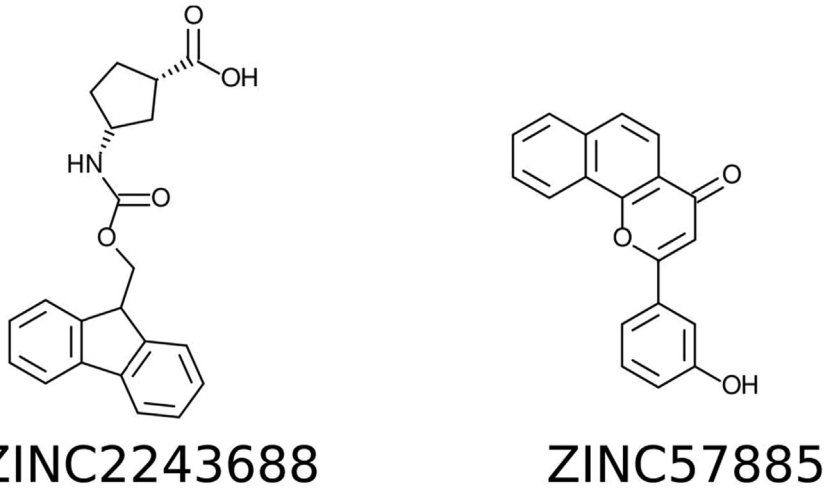

Fig. 3. Chemical structures of molecules selected by virtual screening: (1S,3R)-3-((((9H-Fluoren-9-yl)methoxy)carbonyl)amino)cyclopentanecarboxylic acid (**ZINC2243688**) and 2-phenylbenzo[h]chromen-4-one (**ZINC57885**).

The MG-63 human osteosarcoma cells (CRL1427), A549 human lung adenocarcinoma cells (CCL-185) and MRC-5 human fibroblast (CCL-171) were purchased from ATCC.

2.2. Preparation of the molecular systems

The simulations were based on survivin monomer extracted from dimeric X-ray crystal structure (PDB ID: 1F3H and 1E31). Survivin preparation was done with Molprobity [31]. Water molecules and other ligands were removed. All Asp and Glu residues were considered to have a negative charge and all the Arg and Lys residues were considered to have a positive charge. Histidine tautomers were assigned following the hydrogen bonding pattern. Compounds shown in Fig. 1, taking into account that these molecules have inhibitory capacity measured experimentally against survivin, were taken as active reference ligands. Their structures were sketched using Avogadro molecular editor [32] or

Table 1
Docking score of survivin complexes obtained with Autodock Vina for interface and cavity sites, using 1F3H and 1E31 X-ray structures as targets.

Ligands	Interface		Cavity	
	1F3H	1E31	1F3H	1E31
ABBOTT8	-6.7	-6.9	-8.8	-8.5
LLP3	-7.1	-7.0	-10.8	-9.7
LLP6	-6.3	-6.8	-9.0	-9.1
LLP9	-6.9	-7.2	-9.7	-8.5
LQZ-7B	-7.3	-6.6	-9.3	-9.1
LQZ-7C	-5.7	-7.6	-9.5	-8.5
LQZ-7F	-6.9	-7.1	-8.0	-8.3
S10	-7.0	-7.5	-8.9	-8.1
S12	-6.7	-7.2	-7.9	-8.2
S2	-7.9	-7.9	-9.6	-8.3
ZINC2243688	-7.0	-7.4	-7.5	-8.1
ZINC57885	-7.6	-7.7	-7.9	-8.1

Table 2
Lowest binding free energies of compounds and standard deviation, between parentheses, in the dimerization interface and cavity calculated using MM/GBSA.

Compound	$\Delta G^{MM-GBSA}$ (Kcal/mol)	
	Dimerization interface	Cavity
S12	-11.1 (2.4)	-35.6 (2.5)
LQZ-7F	-17.9 (2.1)	-29.1 (2.8)
ZINC2243688	-13.2 (2.7)	-39.4 (2.9)
ZINC57885	-21.4 (2.4)	-31.4 (3.0)

downloaded from PubChem [33], follow by optimization with PM6 semiempirical method [34], implemented in Mopac [35].

2.3. Molecular docking studies

Molecular docking was carried out to find and score protein-ligand binding poses on a survivin monomer (PDB ID 1F3H:A and 1E31:A) with Autodock Vina [36]. Ligands were docked using a flexible-ligand/rigid-receptor approach. A docking box (30.00 Å × 24.75 Å x 24.00Å, centered in Phe93) was selected to include binding sites mentioned above: dimerization interface and close cavity.

In order to assess the performance of the docking methodology, the area under the receiver operating characteristic curve (ROC AUC) and enrichment factor were calculated. DUD-E [37] was used for generation of decoys from reference active compounds. This server generates 50 decoys for every active provided, with input and output being in SMILES format. The decoys generated were downloaded from ZINC chemical database [38].

For the purpose of applying structure-based virtual screening (SBVS), Sigma Aldrich (Building Blocks) subset was also downloaded from ZINC.

The post-docking analysis included score comparisons of the evaluated compounds respect references and the visualization of the ligand-receptor complexes with Pymol [39] to analyze the potential interactions with the amino acid components of the dimerization interface.

2.4. Molecular dynamics (MD) simulations

The best poses of selected and reference compounds obtained by docking, in the dimerization interface and in the cavity of survivin in monomeric form, were submitted to a MD simulation. The complexes have a negative net charge, sodium cations were added as counterions with Leap module to achieve electroneutrality. The neutralized complexes were immersed in a box of TIP3P waters which extended up to 12 Å from the solute. Receptors were described using the Amber14SB force field [40]. Zinc AMBER force field (ZAFF) [41] was used to describe zinc cation and neighboring residues. Ligands were described using the Generalized Amber Force Field (GAFF) [42] with charges derived from restrained electrostatic potential (RESP) approach, which were calculated with Antechamber module and Gaussian03 [43]. Leap and Antechamber are included in the package AmberTools 16.0 [44].

All MD simulations were run using the NAMD 2.12 software [45]. The van der Waals interaction cutoff distances were set at 12 Å and long-range electrostatic forces were computed using the particle mesh Ewald summation method with a grid size set to 1.0 Å. The 1–4 contributions were multiplied by a factor of 0.83 to match the AMBER force field requirements. Prior to simulations, the systems were subjected to a minimization step: first only the ligand and the water molecules were minimized, then extended to the side chains and, finally to the entire system. MD began by heating from 0 to 300 K over 30 ps and the MD was continued for a total simulation time of 25 ns. Constant temperature (300 K) was maintained using Langevin dynamics with a damping coefficient of 5 ps^{-1}, while pressure was kept constant at 1 atm through the Nosé-Hoover Langevin piston method with a decay period of 200 fs and a damping time constant of 100 fs. A time step of 1 fs was adopted for all simulations,. Bonds involving hydrogen atoms of waters were constrained using the SHAKE algorithm [46]. RMSD values were depicted as a line-style plot to determine the convergence and stability of simulations (Figs. S1, S2 and S5).

2.5. MM/GBSA calculations

Ligand-survivin binding free energies were computed using the MM/GBSA method for all complexes, where the binding free energy is calculated as the difference between the bound and unbound states of protein and ligand [47, 48].

The entropic changes were calculated using quasi-harmonic approximation. The solvation free energy (ΔGsolv) was separated into polar and non-polar contributions. The polar contribution to ΔGsolv was calculated using the generalized Born (GB) model [49] implemented in MMPBSA.py module [50], igb = 3 as selected model. The hydrophobic contribution to ΔG_{solv} was determined using the solvent-accessible surface area (SASA). The protein–ligand binding free energy was calculated using a single trajectory (for ligand, receptor and complex) based on 1000 snapshots taken from the last 10 ns portion (10 ps interval) of the MD simulation trajectories.

For the purpose of obtaining the detailed representation of the ligands/survivin interactions, free energy decomposition analysis was employed to decompose the total binding free energies into ligand–residue pairs. These calculations were performed using a pairwise energy decomposition scheme (idecomp option 3) also with the MMPBSA.py module. In this scheme, interactions are decomposed by specific residue pairs by including only those interactions in which one atom from each of the analyzed residues is participating, following the work of Gohlke et al.[51].

2.6. Cell lines and growth conditions

MG-63 human osteosarcoma cells (CRL1427), A549 human lung adenocarcinoma cells (CCL-185) and MRC-5 human fibroblast (CCL-171) were grown in DMEM containing 10 % FBS, 100 U/mL penicillin, and 100 μg/mL streptomycin at 37 °C in a 5% CO_2 atmosphere. Cells were seeded in a 75 cm^2 flask, and when 70–80 % of confluence was reached, cells were subcultured using 1 mL of TrypLE ™ per 25 cm^2 flask. For experiments, cells were grown in multiwell plates. When cells reached the desired confluence, the monolayers were washed with DMEM and were incubated under different conditions according to the experiments.

2.7. Cell viability assay: 3-(4,5-dimethylthiazol-2-yl)-2,5-diphenyltetrazolium bromide assay

The 3-(4,5-dimethylthiazol-2-yl)-2,5-diphenyltetrazolium bromide (MTT) assay was performed according to Mosmann [52]. Briefly, cells were seeded in a 96-well dish, allowed to attach for 24 h, and treated

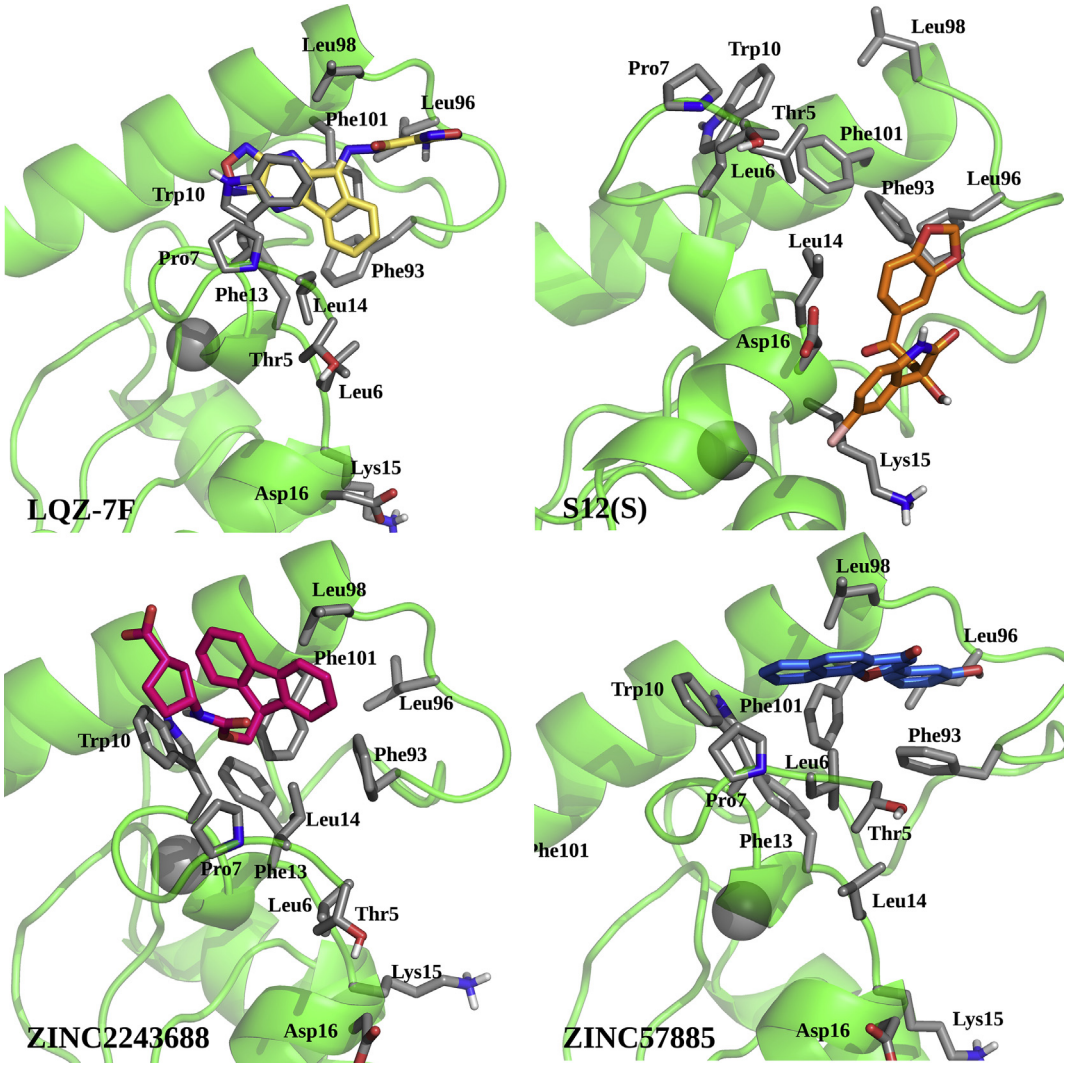

Fig. 4. Poses of selected ligands in the dimerization interface of survivin protein obtained from molecular dynamics.

with different concentrations of compound at 37 °C for 72 h. Afterwards, the medium was changed and the cells were incubated with 0.5 mg/mL MTT under normal culture conditions for 3 h. Cell viability was marked by the conversion of the tetrazolium salt MTT to a colored formazan by mitochondrial dehydrogenases. Color development was measured spectrophotometrically with a microplate reader (model 7530, Cambridge Technology, USA) at 570 nm after cell lysis in DMSO (100 μL per well). Cell viability was plotted as the percentage of the control value.

3. Results and discussion

3.1. Structure-based virtual screening

To validate the docking method, receiver operating characteristic (ROC) curve and enrichment factor (EF) were calculated using Screening Results Analysis Online [53] based on the Autodock Vina score for active ligands and decoys on survivin target (PDB ID: 1F3H). ROC AUC value was 0.898, which shows a good docking performance. In general, an AUC of 0.5 suggests no discrimination (i.e., ability to discriminate active molecules from decoys), while an area of 1 reflects a perfectly accurate test. Enrichment factors were 4.7 ($EF_{\%2}$)/7.4 ($EF_{\%5}$). ROC curve is showed in Fig. S3. Decoys and reference ligands with their scores are listed in Table SI of Supporting Information.

It should be clarified that for **S12** and related compounds, based on literature search, it is not established which of the enantiomers is the active against survivin, and the drug is marketed as racemic mixture. For this reason both enantiomers were tested. Based on molecular dynamics results, see below, only the S enantiomer was included in ROC curve analysis.

Results analysis shows that the best poses of ligands and decoys locate mainly in a cavity, which is composed principally by residues Arg18, Glu40, Phe86, Val89 and Lys91. This location was also observed for the compounds reported by Qi et al. [26], **LQZ-7** and its analogs which had been reported as located in another site, the dimerization interface. A detailed description of both sites is depicted in Fig. 2. It should be notice that virtual screening was carried out with one of the monomers, chain A. Another chain has been included in the figure to facilitate the description.

A virtual screening was performed on Sigma Aldrich catalog, included in ZINC database, with the aim of identifying new potential inhibitors of human survivin. Two compounds were selected from those that showed better affinity according to the virtual screening results, even outperforming the reference compounds, based on observation and feasibility of acquisition: 2-(3-hydroxyphenyl)benzo[h]chromen-4-one **(ZINC57885)** and (1S,3R)-3-((((9H-Fluoren-9-yl) methoxy)carbonyl) amino)cyclopentanecarboxylic acid **(ZINC2243688)** (see Fig. 3).

In order to compare and analyze the interaction of reference compounds and selected compounds with the cavity and the dimerization interface, dockings limited to each of these regions were performed.

The results of molecular docking showed that the best scored poses,

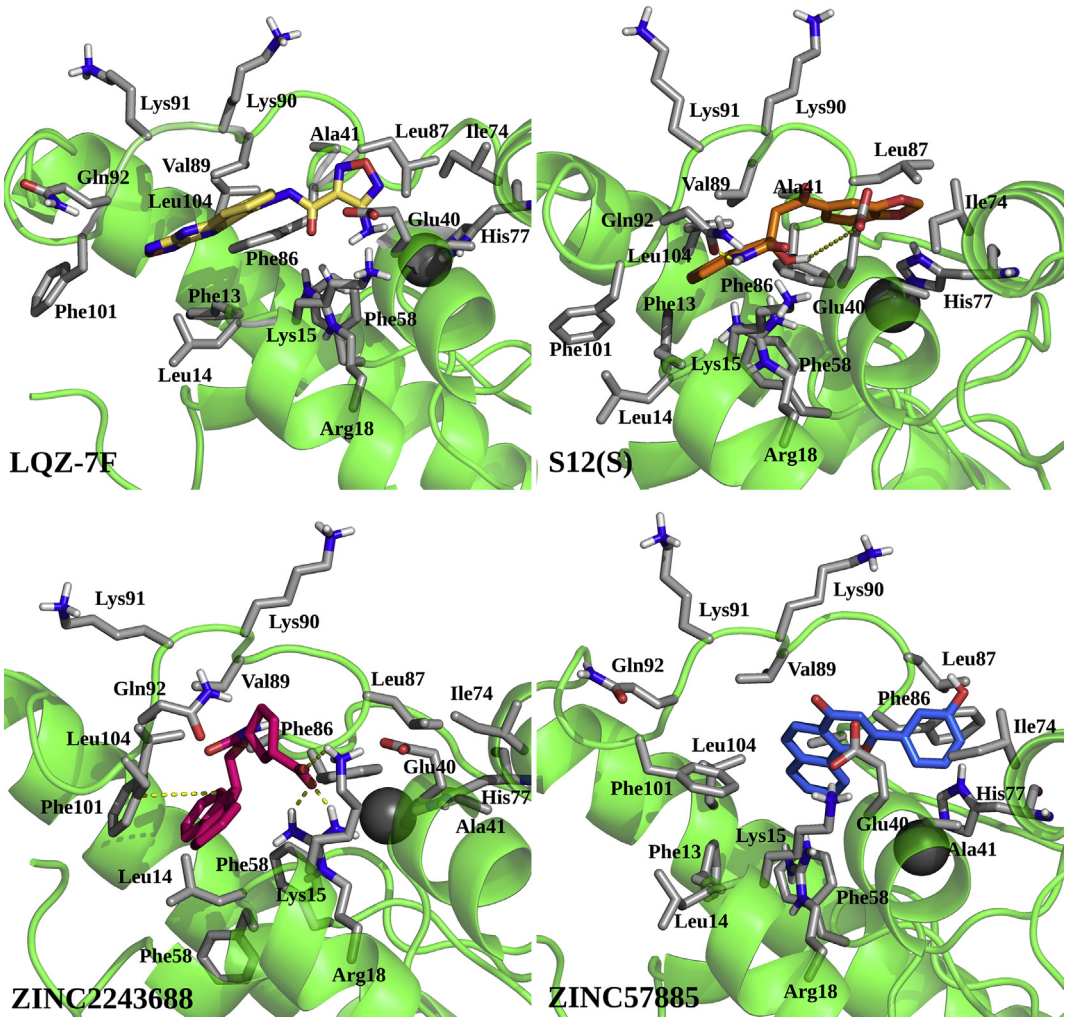

Fig. 5. Poses of selected ligands in cavity of survivin protein obtained from molecular dynamics.

for the selected and references compounds, were preferentially positioned in cavity (Table 1).

In addition, to analyze if conformational variations in the receptor could change the trend and increase the number of poses located in the dimerization interface, rotamers were generated with Autodock Vina for residues Trp10, Phe13, Phe58, Phe86, Val89, Phe93, Glu94, Leu96, Gln92, Leu98 and, Phe101. Except for **ZINC57885,** which was more inserted in the cavity (pose then discarded based on MM/GBSA energy results), the rest of ligands showed no significant changes in location and Autodock Vina scores with respect to rigid receptor.

An additional crystalline structure of human survivin (PDB ID: 1E31) was used also as target because it revealed some differences respect 1F3H, in particular Gln92, and this could affect the entrance of the ligand in the cavity. It resulted that there were no appreciable differences between the targets, both in Autodock Vina score and in the structures of the generated poses, so it was decided to continue only with 1F3H X-ray structure.

3.2. Molecular dynamics and binding energies

MD simulation studies were then performed to study the binding modes of these compounds. Considering the high computational cost to run MD simulation, this technique was applied on **LQZ-7F** and **S12**, which were taken as "extreme" ligand references, located by authors in the dimerization interface and the cavity sites, respectively. **ZINC57885** and **ZINC2243688** were also studied with MD. Some poses, including the best scored from Autodock Vina of each region, were selected and submitted to a MD with 25ns of molecular dynamic simulation. From frames extracted from last 10ns of these trajectories, and using the MM-GBSA model, binding energies were estimated for these ligands, see Table 2. The most stable poses found for the dimerization interface and cavity sites are shown in Fig. 4 and Fig. 5, respectively. It is observed that in both the reference ligands and in the compounds selected by virtual screening, the binding energy is more favorable in the cavity with respect to the dimerization interface. This result agrees with the trend obtained by docking.

For the dimerization interface, energy contributions per residue to the energy binding using MM/GBSA are shown in Fig. 6, this allows an interpretation of the contributions to the total interaction energy (Table SII shows mean distance between ligands and residues over the last 10 ns of molecular dynamic simulation).

Interactions established by **LQZ-7F** and survivin were in agreement with reported by Qi et al. [26]: π-π stacking and hydrophobic interaction between the tetracyclic furazanopyrazine ring of **LQZ-7F** and the hydrophobic residues Trp10, Phe93, Leu98 and Phe101, the last two considered core residues of the dimerization interface; H-bond between the primary amine group of **LQZ-7F** and Glu94 of surviving. In our results, an additional interaction with Leu96 is observed.

ZINC57885 and **ZINC2243688** binding modes analysis revealed interactions between ligands with the core residues of the dimerization interface: the naphthyl and phenyl groups of **ZINC57885** and the fluorenyl ring system of **ZINC2243688** establish π-π stacking interactions

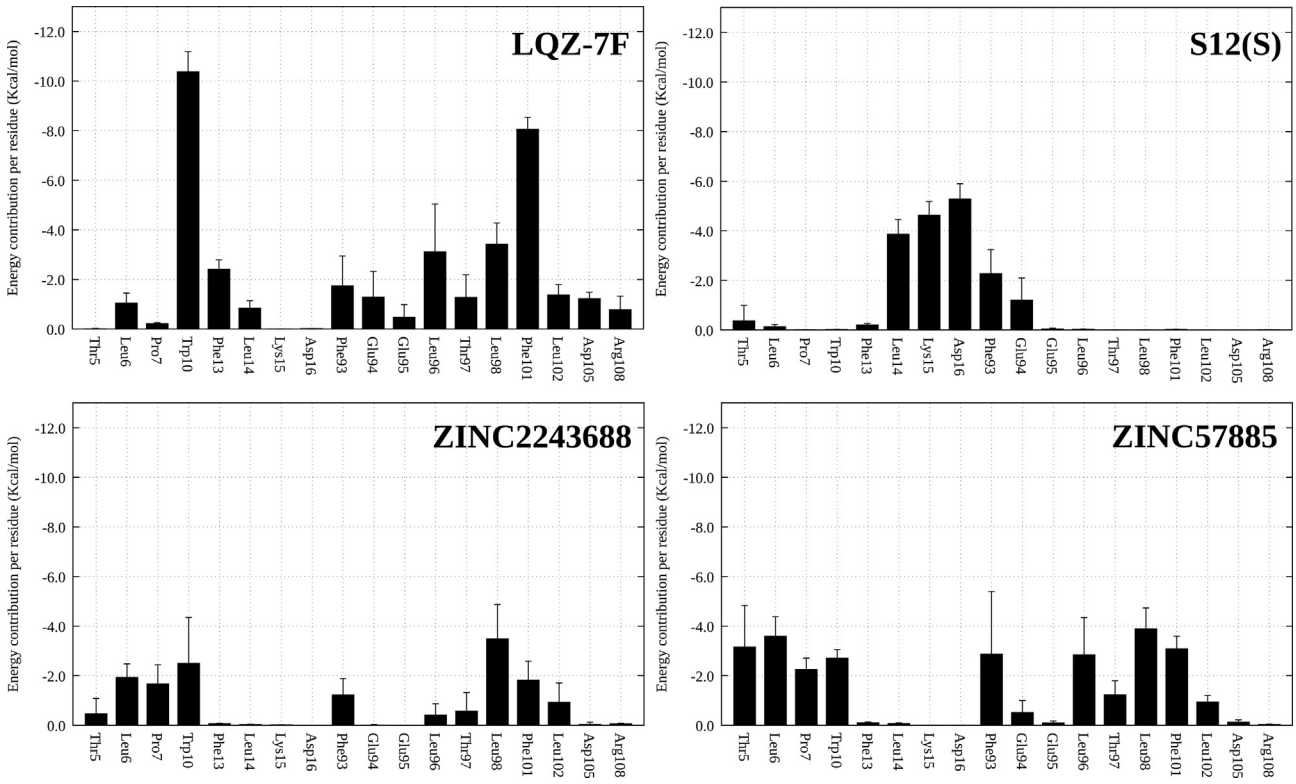

Fig. 6. Plot of MM/GBSA binding free energy contribution per residue of the complexes in the dimerization interface site, calculated with MMPBSA.py.

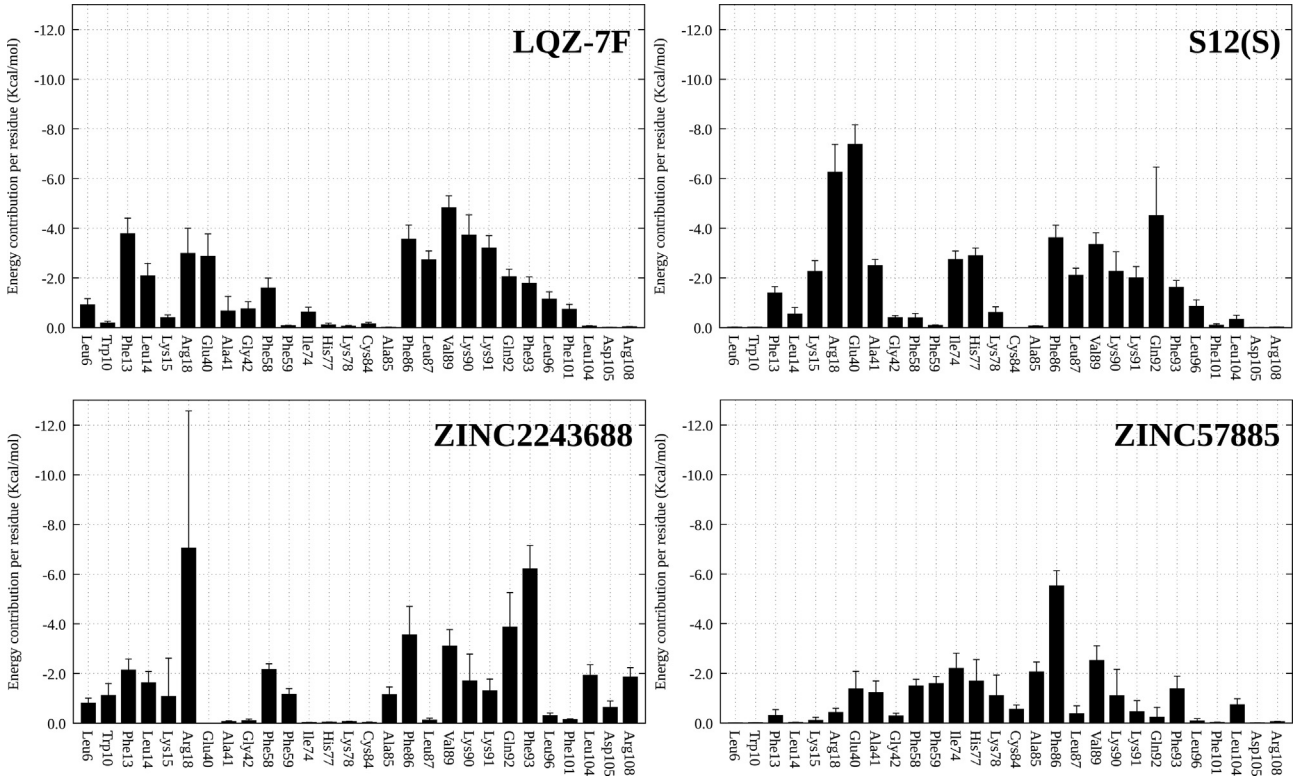

Fig. 7. Plot of MM/GBSA binding free energy contribution per residue of the complexes in the dimerization interface site, calculated with MMPBSA.py.

with Phe93 and Phe101, and π-alkil with Leu98. These molecules also interact with residues Trp10 and Leu96.

In the cavity, contributions per residue to the energy binding were also calculated and are showed in Fig. 7 (Table SIII shows mean distance between ligands and residues over the last 10 ns of molecular dynamic simulation). The ligands, with the exception of **ZINC57885**, are stabilized by hydrogen bond interactions (conventional or carbon-hydrogen bond) with one or more of residues Arg18, Glu40, Val89 or Gln92.

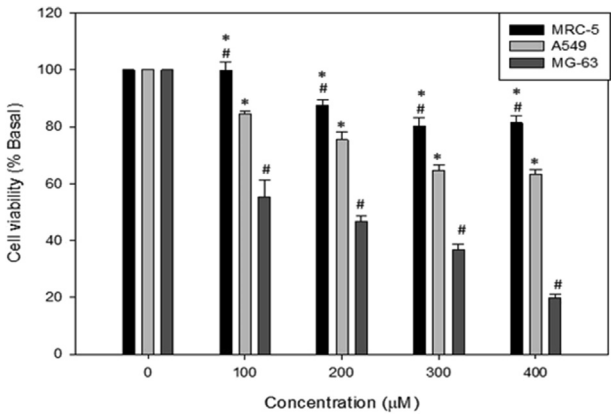

Fig. 8. Effects of ZINC2243688 on cell viability of human normal fibroblast (MRC-5), human lung adenocarcinoma (A549) and human bone osteosarcoma (MG-63).

Also, only for **ZINC2243688**, a hydrogen bond interaction is observed with Phe93 through the carboxylic acid.

A special mention deserves **S12** case. Poses of both **S12** enantiomers were obtained by docking and subjected to molecular dynamics and MM/GBSA calculations. S enantiomer showed to be 21.3 kcal mol^{-1} more stable than R enantiomer in the cavity. According to the energy decomposition per residue, see Fig. S4, **S12(S)** establishes interactions by hydrogen bond with residues Arg18, Glu40, and Gln92. However, **S12(R)** is unable to establish interactions with Arg18 and Glu40 because hydroxyl group of oxindole is located away from these residues and opposite in the plane. Hydrophobic contacts with side chains of Phe13, Phe86, Val89, Leu96, and Phe93 do not change significantly between both enantiomers. Mean distances between this residues and enantiomers, showed in Table SIII, agree with these observations. Furthermore, Berezov et al. [27] have experimentally verified that **S12** is not capable of interacting with survivin mutants (F86A and V89T). To evaluate if the modeled system complied with experimental observations, both mutated survivin were prepared and subjected to the same protocol (minimization, heating, equilibration). The binding energy of **S12(S)** with the mutated survivins F86A and V89T was less favorable compared to the WT protein ($\Delta\Delta G_{bind}$ 13.7 kcal mol^{-1} and 7.5 kcal mol^{-1} respectively), which agrees with the experimental results. Based on energy decomposition per residue, see Fig. S6, the interactions most affected by these mutations were hydrogen bonds: magnitude of such interactions with Arg18, Glu40 Gln92 decrease respect to WT. In both cases, the oxindole group undergoes a position change. On the other hand, interaction pattern of **S12(S)** with hydrophobic residues of survivin-F86A was similar to that observed for survivin-WT, with the exception of Phe93 in which a π-π stacking interaction is observed with the 3-hydroxyindole. In survivin-V89T case, **S12(S)** shows less interaction with most of hydrophobic residues, with the exception of Phe86, which establishes a strong π-π stacking interaction with benzo [1, 3]-dioxolyl group.

3.3. Cytotoxicity assays

In order to evaluate the antitumor activity and selectivity of the selected compounds and with the intention to corroborate the predicted effect from the in silico studies, the human tumor cell lines with over expression of survivin A549 (lung) and MG-63 (bone) and the non-cancerous cell line (MRC-5) were selected. They were treated with **ZINC57885** and **ZINC2243688** at different concentrations to compare the sensitivity.

Fig. 8 shows the anticancer activity of **ZINC2243688** on three cell lines. The data presented herein show a cytotoxic effect of **ZINC2243688** in a concentration-dependent manner from 100 to 400 μM on A549 and MG-63 with statistically significant differences versus the control ($p < 0.01$).

Nevertheless, this compound only shows slight cytotoxicity effects on normal MRC-5 cells suggesting that has a very good correlation in the effects over normal and tumor cells. In this sense, it was observed that cell lines with overexpression of survivin were much more sensitive to the deleterious effect of the treatment with **ZINC2243688** respect to the non-cancerous line.

On the other hand, it should be clarify that problems with **ZINC057885** solubility in the cell culture medium was a main factor that limited the studies carried out with this compound (Results are not shown).

4. Conclusions

In this work, we have identified a potential lead inhibitor (**ZINC2243688**) that could bind to survivin in a cavity close to the dimerization interface. These findings were achieved using docking score and MM/GBSA binding energies using trajectories of molecular dynamics. Using these techniques also, it was observed that interactions between test ligands and survivin dimerization interface are possibly less favorable with respect interactions with this cavity.

The conformational analysis and free energy profile per residue calculated for **S12** with survivin correlated with the experimental results observed by Berezov et al. [27] In addition, based on the energy results, the S enantiomer of **S12** is proposed as the active isomer against survivin.

On the other hand, our results suggest that the interaction of **LQZ-7** and its analogues with the survivin possibly occurs also in the cavity. This result is in contrast to what was predicted by Qi et al. [26] This difference possibly is due to the fact that these authors restricted the docking analysis space to the dimerization interface region. It should be noted that the energy difference between both locations (cavity and dimerization interface) is not high respect to its standard error, so further research should be carried out with other techniques to be conclusive.

Besides, **ZINC2243688** diminished the cell viability on bone and lung cancer cells showing a higher selectivity toward tumor than normal cells. In this way, it was observed that cell lines that overexpressed survivin (MG-63, A549) was much more sensitive to the deleterious action of **ZINC2243688** compared to the normal cell line (MCR-5) suggesting the importance of survivin as molecular target in cancer therapies.

Declarations

Author contribution statement

Patricia Quispe: Performed the experiments; Analyzed and interpreted the data.

Martin Lavecchia, Ignacio E. León: Conceived and designed the experiments; Analyzed and interpreted the data; Wrote the paper.

Funding statement

This work was partly supported by UNLP (11X/690), CONICET (PIP 0034), and ANPCyT (PICT 2016-1574) from Argentina.

Competing interest statement

The authors declare no conflict of interest.

Additional information

Supplementary content related to this article has been published online at https://doi.org/10.1016/j.heliyon.2019.e02238.

Acknowledgements

IEL and MJL are members of the Carrera de Investigador, CONICET,

Argentina. PAQ has a fellowship from CIC, Argentina. We gratefully acknowledge the support of NVIDIA Corporation with the donation of the Titan X Pascal GPU used for this research.

References

[1] S. Fulda, D. Vucic, Targeting IAP proteins for therapeutic intervention in cancer, Nat. Rev. Drug Discov. 11 (2012) 109–124.
[2] G. Ambrosini, C. Adida, D.C. Altieri, A novel anti-apoptosis gene, survivin, expressed in cancer and lymphoma, Nat. Med. 3 (1997) 917–921.
[3] N.K. Sah, C. Seniya, Survivin splice variants and their diagnostic significance, Tumour Biol J Int Soc Oncodevelopmental Biol Med 36 (2015) 6623–6631.
[4] L. Chantalat, D.A. Skoufias, J.P. Kleman, et al., Crystal structure of human survivin reveals a bow tie-shaped dimer with two unusual alpha-helical extensions, Mol. Cell 6 (2000) 183–189.
[5] F. Li, G. Ambrosini, E.Y. Chu, et al., Control of apoptosis and mitotic spindle checkpoint by survivin, Nature 396 (1998) 580–584.
[6] M.A. Verdecia, H. Huang, E. Dutil, et al., Structure of the human anti-apoptotic protein survivin reveals a dimeric arrangement, Nat. Struct. Biol. 7 (2000) 602–608.
[7] F. Li, E.J. Ackermann, C.F. Bennett, et al., Pleiotropic cell-division defects and apoptosis induced by interference with survivin function, Nat. Cell Biol. 1 (1999) 461–466.
[8] D.C. Altieri, Survivin, cancer networks and pathway-directed drug discovery, Nat. Rev. Cancer 8 (2008) 61–70.
[9] P.K. Jaiswal, A. Goel, R.D. Mittal, Survivin: a molecular biomarker in cancer, Indian J. Med. Res. 141 (2015) 389–397.
[10] A.I. Sarela, R.C. Macadam, S.M. Farmery, et al., Expression of the antiapoptosis gene, survivin, predicts death from recurrent colorectal carcinoma, Gut 46 (2000) 645–650.
[11] K. Jha, M. Shukla, M. Pandey, Survivin expression and targeting in breast cancer, Surg Oncol 21 (2012) 125–131.
[12] H. Li, J.Y. Niederkorn, S. Neelam, H. Alizadeh, Downregulation of survivin expression enhances sensitivity of cultured uveal melanoma cells to cisplatin treatment, Exp. Eye Res. 83 (2006) 176–182.
[13] H. Kojima, M. Iida, Y. Yaguchi, et al., Enhancement of Cisplatin sensitivity in squamous cell carcinoma of the head and neck transfected with a survivin antisense gene, Arch. Otolaryngol. Head Neck Surg. 132 (2006) 682–685.
[14] K. Yonesaka, K. Tamura, T. Kurata, et al., Small interfering RNA targeting survivin sensitizes lung cancer cell with mutant p53 to adriamycin, Int. J. Cancer 118 (2006) 812–820.
[15] M.S. Coumar, F.-Y. Tsai, J.R. Kanwar, et al., Treat cancers by targeting survivin: just a dream or future reality? Cancer Treat Rev. 39 (2013) 802–811.
[16] D.N. Church, D.C. Talbot, Survivin in solid tumors: rationale for development of inhibitors, Curr. Oncol. Rep. 14 (2012) 120–128.
[17] Z.-F. Liu, Z.-Q. Liang, L. Li, et al., MiR-335 functions as a tumor suppressor and regulates survivin expression in osteosarcoma, Eur. Rev. Med. Pharmacol. Sci. 20 (2016) 1251–1257.
[18] D.C. Talbot, M. Ranson, J. Davies, et al., Tumor survivin is downregulated by the antisense oligonucleotide LY2181308: a proof-of-concept, first-in-human dose study, Clin Cancer Res Off J Am Assoc Cancer Res 16 (2010) 6150–6158.
[19] A. Rauch, D. Hennig, C. Schäfer, et al., Survivin and YM155: how faithful is the liaison? Biochim. Biophys. Acta 1845 (2014) 202–220.
[20] Z. Zhang, Y. Zhang, J. Lv, J. Wang, The survivin suppressant YM155 reverses doxorubicin resistance in osteosarcoma, Int. J. Clin. Exp. Med. 8 (2015) 18032–18040.
[21] T. Nakahara, A. Kita, K. Yamanaka, et al., YM155, a novel small-molecule survivin suppressant, induces regression of established human hormone-refractory prostate tumor xenografts, Cancer Res. 67 (2007) 8014–8021.
[22] F. Li, Discovery of survivin inhibitors and beyond: FL118 as a proof of concept, Int Rev Cell Mol Biol 305 (2013) 217–252.
[23] L.R. VanSchoiack, V.I. Shubayev, R.R. Myers, et al., In vivo evaluation of quantitative percussion diagnostics for determining implant stability, Int. J. Oral Maxillofac. Implant. 28 (2013) 1286–1292.
[24] L.N. Makley, J.E. Gestwicki, Expanding the number of "druggable" targets: non-enzymes and protein-protein interactions, Chem. Biol. Drug Des. 81 (2013) 22–32.
[25] C.H.A. Cheung, C.-C. Huang, F.-Y. Tsai, et al., Survivin – biology and potential as a therapeutic target in oncology, OncoTargets Ther. 6 (2013) 1453–1462.
[26] J. Qi, Z. Dong, J. Liu, et al., Effective targeting of the survivin dimerization interface with small-molecule inhibitors, Cancer Res. 76 (2016) 453–462.
[27] A. Berezov, Z. Cai, J.A. Freudenberg, et al., Disabling the mitotic spindle and tumor growth by targeting a cavity-induced allosteric site of survivin, Oncogene 31 (2012) 1938–1948.
[28] S.N. Chettiar, J.V. Cooley, I.-H. Park, et al., Design, synthesis and biological studies of survivin dimerization modulators that prolong mitotic cycle, Bioorg. Med. Chem. Lett 23 (2013) 5429–5433.
[29] M.D. Wendt, C. Sun, A. Kunzer, et al., Discovery of a novel small molecule binding site of human survivin, Bioorg. Med. Chem. Lett 17 (2007) 3122–3129.
[30] I.-H. Park, C. Li, Dynamic ligand-induced-fit simulation via enhanced conformational samplings and ensemble dockings: a survivin example, J. Phys. Chem. B 114 (2010) 5144–5153.
[31] V.B. Chen, W.B. Arendall, J.J. Headd, et al., MolProbity: all-atom structure validation for macromolecular crystallography, Acta Crystallogr D Biol Crystallogr 66 (2010) 12–21.
[32] M.D. Hanwell, D.E. Curtis, D.C. Lonie, et al., Avogadro: an advanced semantic chemical editor, visualization, and analysis platform, J. Cheminf. 4 (2012) 17.
[33] S. Kim, P.A. Thiessen, E.E. Bolton, et al., PubChem substance and compound databases, Nucleic Acids Res. 44 (2015) D1202–D1213.
[34] J.J. Stewart, Optimization of parameters for semiempirical methods V: modification of NDDO approximations and application to 70 elements, J. Mol. Model 13 (2007) 1173–1213.
[35] J.J. Stewart, MOPAC: a semiempirical molecular orbital program, J. Comput. Aided Mol. Des. 4 (1990) 1–103.
[36] O. Trott, A.J. Olson, AutoDock Vina: improving the speed and accuracy of docking with a new scoring function, efficient optimization and multithreading, J. Comput. Chem. 31 (2010) 455–461.
[37] M.M. Mysinger, M. Carchia, J.J. Irwin, B.K. Shoichet, Directory of useful decoys, enhanced (DUD-E): better ligands and decoys for better benchmarking, J. Med. Chem. 55 (2012) 6582–6594.
[38] J.J. Irwin, B.K. Shoichet, ZINC – a free database of commercially available compounds for virtual screening, J. Chem. Inf. Model. 45 (2005) 177–182.
[39] W.L. DeLano, PyMOL, 2002.
[40] J.A. Maier, C. Martinez, K. Kasavajhala, et al., ff14SB: improving the accuracy of protein side chain and backbone parameters from ff99SB, J. Chem. Theory Comput. 11 (2015) 3696–3713.
[41] M.B. Peters, Y. Yang, B. Wang, et al., Structural survey of zinc containing proteins and the development of the zinc AMBER force field (ZAFF), J. Chem. Theory Comput. 6 (2010) 2935–2947.
[42] J. Wang, R.M. Wolf, J.W. Caldwell, et al., Development and testing of a general amber force field, J. Comput. Chem. 25 (2004) 1157–1174.
[43] Frisch Mj, G.W. Trucks, Schlegel Hb, et al., Gaussian 03, revision C. 02, 2008.
[44] D.A. Case, T.A. Darden, T.E. Cheatham III, et al., AmberTools 16, University of California, San Francisco, 2016.
[45] J.C. Phillips, R. Braun, W. Wang, et al., Scalable molecular dynamics with NAMD, J. Comput. Chem. 26 (2005) 1781–1802.
[46] J.-P. Ryckaert, G. Ciccotti, H.J.C. Berendsen, Numerical integration of the cartesian equations of motion of a system with constraints: molecular dynamics of n-alkanes, J. Comput. Phys. 23 (1977) 327–341.
[47] J. Srinivasan, T.E. Cheatham, P. Cieplak, et al., Continuum solvent studies of the stability of DNA, RNA, and Phosphoramidate−DNA helices, J. Am. Chem. Soc. 120 (1998) 9401–9409.
[48] Y.N. Vorobjev, J. Hermans, ES/IS: estimation of conformational free energy by combining dynamics simulations with explicit solvent with an implicit solvent continuum model, Biophys. Chem. 78 (1999) 195–205.
[49] W.C. Still, A. Tempczyk, R.C. Hawley, T. Hendrickson, Semianalytical treatment of solvation for molecular mechanics and dynamics, J. Am. Chem. Soc. 112 (1990) 6127–6129.
[50] B.R. Miller, T.D. McGee, J.M. Swails, et al., MMPBSA.py: an efficient program for end-state free energy calculations, J. Chem. Theory Comput. 8 (2012) 3314–3321.
[51] A. Metz, C. Pfleger, H. Kopitz, et al., Hot spots and transient pockets: predicting the determinants of small-molecule binding to a protein-protein interface, J. Chem. Inf. Model. 52 (2012) 120–133.
[52] T. Mosmann, Rapid colorimetric assay for cellular growth and survival: application to proliferation and cytotoxicity assays, J. Immunol. Methods 65 (1983) 55–63.
[53] C. Empereur-Mot, J.-F. Zagury, M. Montes, Screening explorer–an interactive tool for the analysis of screening results, J. Chem. Inf. Model. 56 (2016) 2281–2286.